

Preparation and Characterization of Poly(butylene succinate) Bionanocomposites Reinforced with Cellulose Nanofiber Extracted from *Helicteres isora* Plant

Jithin Joy^{1,2,3}, Cintil Jose³, Srirama B. Varanasi⁴, Lovely Mathew P.^{2,3}, Sabu Thomas² and Srikanth Pilla^{1,5*}

¹Department of Automotive Engineering, Clemson University, SC, 29607 USA

²International and Inter University Centre for Nanoscience and Nanotechnology and School of Chemical Sciences, Mahatma Gandhi University, Kottayam, Kerala, 686 560, India

³Department of Chemistry, Newman College, Thodupuzha, Kerala, 685 585, India

⁴Bloomfield Hills High School, Bloomfield Hills, MI, 48302, USA

⁵Department of Materials Science and Engineering, Clemson University, SC, 29607 USA

Received June 17, 2016; Accepted September 13, 2016

ABSTRACT: Isora nanofibers (INF) were produced by a combined thermal-chemical-mechanical method from *Helicteres isora* plant. The resulting fibers were analyzed using transmission electron microscopy and scanning electron microscopy, which showed a network-like structure with a length of 600 nm, width of 50 nm and an aspect ratio of 12. Fourier transform infrared spectroscopy indicated that chemical treatments progressively removed noncellulosic constituents. X-ray diffraction analysis revealed that crystallinity increased with successive chemical treatments. Using the synthesized isora nanofibers, poly(butylene succinate) (PBS)-based biodegradable nanocomposites were prepared. The nanocomposites were processed using a Brabender twin-screw compounder and an injection molding machine. Effects of INF on the mechanical properties of nanocomposites were investigated. Tensile and flexural moduli of PBS-INF nanocomposites showed an increase with increase in INF content owing to the network formation of the nanofibers in the PBS matrix, whereas toughness and strain-at-break exhibited the opposite trend. Tensile and flexural strengths showed an increase up to 1.5 phr of INF loading, beyond which they were observed to decline owing to agglomeration of INF. Theoretically predicted tensile strength and Young's modulus were found to increase with INF content; however, there existed a mismatch between theoretical predictions and experimental observations.

KEYWORDS: Poly(butylene succinate), nanocellulose fiber, nanocomposite, *Helicteres isora*

1 INTRODUCTION

Plastics, due to their versatility, ease of manufacture, and comparatively lower cost, coupled with unique thermal, mechanical, and electrical properties, are used in day-to-day life for an expanding range of applications from disposable utensils to space shuttles. According to targeted applications, polymer properties are enhanced and/or modulated by the addition of diverse kinds of fillers. The non-biodegradable nature of these plastics (pristine/composite) has led to the generation of infinite amounts of solid waste. Hence, researchers across the world are working on developing sustainable plastics that are biodegradable

or compostable under simulated aging conditions. Poly(butylene succinate) (PBS) is among the most promising biodegradable aliphatic polyesters. PBS can be synthesized by poly-condensation of 1,4-butanediol with succinic acid [1]. Compared to other biodegradable polymers, PBS possesses superior mechanical and thermal properties, good processability, and high chemical resistance [2, 3]. PBS has a melting point in the range of 90–120 °C, glass transition temperature in the range of –45 to –10 °C (between that of polyethylene (PE) and polypropylene (PP)), tensile strength between that of PE and PP, and stiffness between that of low-density polyethylene (LDPE) and of high-density polyethylene (HDPE) [4]. Moreover, PBS undergoes biodegradation during disposal in compost, moist soil, fresh water (by activated sludge), and seawater [5]. However, compared to synthetic plastics, PBS has inferior mechanical properties, which

*Corresponding author: spilla@clemson.edu

DOI: 10.7569/JRM.2016.634128

limits its widespread use. Use of non-biodegradable synthetic fillers can improve the properties, but renders the composite non-biodegradable. Hence, to increase the use of PBS an appropriate reinforcement strategy, which enhances the properties (e.g., mechanical properties) while maintaining the highly sought-after biodegradability, is essential.

Replacing traditional synthetic reinforcement fibers with natural fibers (e.g., natural cellulose fibers) [6–8] is an attractive proposition to solve the problem mentioned above. Use of such completely biodegradable composites in fields such as the automotive, packaging, and furniture industries could significantly reduce the amount of non-degradable wastes. Various PBS-based green composites reinforced with a variety of biofibers are reported [1, 5, 9–20]. Among the diverse biofibers reported, cellulose, a readily available renewable and biodegradable biopolymer, with high mechanical strength, low density, chemical stability, and ease of derivatization, is being intensely researched to fabricate biodegradable composites [3–5]. Cellulose extracted from different sources, including sugar beet [21–27], potato tuber cell [28, 29], lemon and maize [30], coir [15, 31–36], banana [37–41], as well as various other renewable resources [42–52], exhibited varying reinforcing ability, indicating the strong correlation of the aspect ratio, crystallinity, morphology, and properties of cellulose with the raw material and the employed extraction process [53].

However, all these studies use micro- or macro-scale fillers, which in spite of enhancing the mechanical properties, needed to be added at high volume ratios to achieve the desired strengths. Moreover, while the addition of most of the reinforcement fibers to PBS resulted in the enhancement of tensile properties [1, 9–16, 18–20], addition of certain natural fibers such as starch [43], cellulose filler [43], rice husk flour [44], wood flour [17, 44], and lignin [5] led to a decline in the tensile strength. Other mechanical properties, including elastic modulus (except in the case of basalt fiber [45]), flexural strength, etc., also showed significant enhancement upon addition of biofibers-based fillers. It is worth noting that the optimal filler loading in all these studies is in the range of 10–40% (high loading), except in the case of cellulose whiskers [46], due to the micro/macro nature of the fillers used. Nanodimensional fillers, due to their unique structure and properties, could enhance the properties even at a lower loading. It is interesting to note that while various PBS-based nanocomposites containing diverse filler systems have been investigated, reinforcement with bio-based nanofibers, particularly nanocellulose, are rare. One particular example is by Lin *et al.*, where they observed a significant enhancement of mechanical performance and crystalline properties of PBS

matrix when reinforced with cellulose whisker and platelet-like starch nanocrystal [46].

In the present study, we extracted isora nanofiber (INF) from *Helicteres isora* plant by using a combined thermal-chemical-mechanical method. The method yielded nanosized INF fibers. INF was characterized using scanning electron microscopy (SEM), transmission electron microscopy (TEM), Fourier transform infrared (FTIR) spectroscopy, X-ray diffraction analysis (XRD) and thermogravimetric analysis (TGA). We also fabricated PBS-based nanocomposites using these INF fibers and investigated their morphology, microstructure, and mechanical properties. The nano dimensions of prepared INFs enabled the nanocomposite to exhibit enhanced mechanical properties with INF loading of only 1.5%, an order of magnitude reduction compared to typical micro/macro biofillers. Finally, some analytical models were used to predict theoretical tensile strength and Young's modulus of the nanocomposites and compared with experimental results to gain a better understanding of the interactions between PBS and INF.

2 EXPERIMENTAL

2.1 Materials

Polybutylene succinate (PBS) (melt flow index: 25g/10min; density: 1.20–1.28g/cm³; melting point: 114 °C) was purchased from Shanghai Yuhan Biotechnology Co., China. INF was extracted from the barks of *Helicteres isora* plant collected from the forests of South India. Analytical grade reagents—hydrogen peroxide, sodium hydroxide and oxalic acid—were used. A homogenizer of type IKA®T25 digital Ultra-Turrax and a laboratory autoclave (with 25 psi pressure) were also used for preparation of INF.

2.2 Methods

2.2.1 Preparation of INF

Helicteres isora (family: Sterculiaceae) is a lignocellulosic rich fiber (tensile strength ~ 500 MPa, elastic modulus of 26.3 GPa, and elongation-at-break ~ 2.5%) [48]. Isora fibers were chopped into short length of about 0.5–1 cm, treated with 2 wt% NaOH solution in an autoclave in the ratio of 1:10 (fiber:solution, w/v), and kept at a pressure of 20 psi and temperature range of 110–120 °C for a duration of one hour. Thoroughly washed and dried fibers were then bleached with hydrogen peroxide (H₂O₂) using a solution of 30% (v/v) H₂O₂ and 4% (w/v) NaOH in a water bath at 60 °C in the ratio of 1:20 (fiber:solution, w/v) with constant stirring for 90 min. The bleached isora fibers were washed with distilled

water until the solution reached the pH value of 7. Isora fibers were oven-dried at 60 °C for 12 hours, and the H₂O₂ bleaching procedure was then repeated three times [31, 47]. The bleached fibers were then treated with 10 vol% oxalic acid in an autoclave under pressure of 20 psi and at a temperature of 110 °C for one hour. Immediate release of the pressure led to defibrillation of the fibers [34], and this acid treatment process was repeated four times. Acid-hydrolyzed solution, containing fibers, was homogenized for 20 min at 12,000 rpm using an IKA®T25 Ultra-Turrax digital homogenizer, following which the suspension was kept in an oven at 80 °C till it was fully dry [48]. A schematic representation of the experimental procedure for preparation of INF is given in Figure 1.

2.2.2 Preparation of Nanocomposites

Melt mixing of PBS with different INF loadings (0.5, 1, 1.5 and 2 parts per hundred parts of polymer resin [phr]), was performed in a Brabender twin-screw compounder (GmbH & Co. KG, Duisburg, Germany), at 140 °C for 9 min at a screw speed of 90 rpm. The extruded strand was pelletized and dried at 80 °C for 24 hours. Extruded pellets were injection molded into tensile (ISO 20753 A₁₂) and flexural (ISO 178) test bars using a micro injection molding machine (DSM

Xplore, Netherlands) at 140 °C and an injection pressure of 1200 psi.

2.3 Characterization

2.3.1 Isora Nanofiber

Chemical composition of raw isora fiber and fibers at each treatment was measured as per the Technical Association of Pulp and Paper Industry (TAPPI) standard. α -Cellulose and hemicellulose content were determined by TAPPI T19 m-54 method, while lignin content was analyzed by TAPPI-T222 om-88 method [7, 49]. A minimum of five samples were tested for each material, and average values were calculated. A fixed amount of INF suspended in water was dried up to constant weight at 105 °C, and the yield of INFs was calculated by using an electronic analytical balance (Mettler Toledo ML204/actual scale interval = 0.1 mg).

Scanning electron microscopy (SEM) (JEOL JSM-820 model) was used to observe the effect of different chemical treatments on the surface morphology of isora fibers. The samples were coated with gold using a vacuum sputter coater (model SC500) to avoid subsequent charging before measurement by SEM, with the accelerating voltage being 20 kV. A JEOL JEM 2100 high resolution transmission electron microscope (TEM)

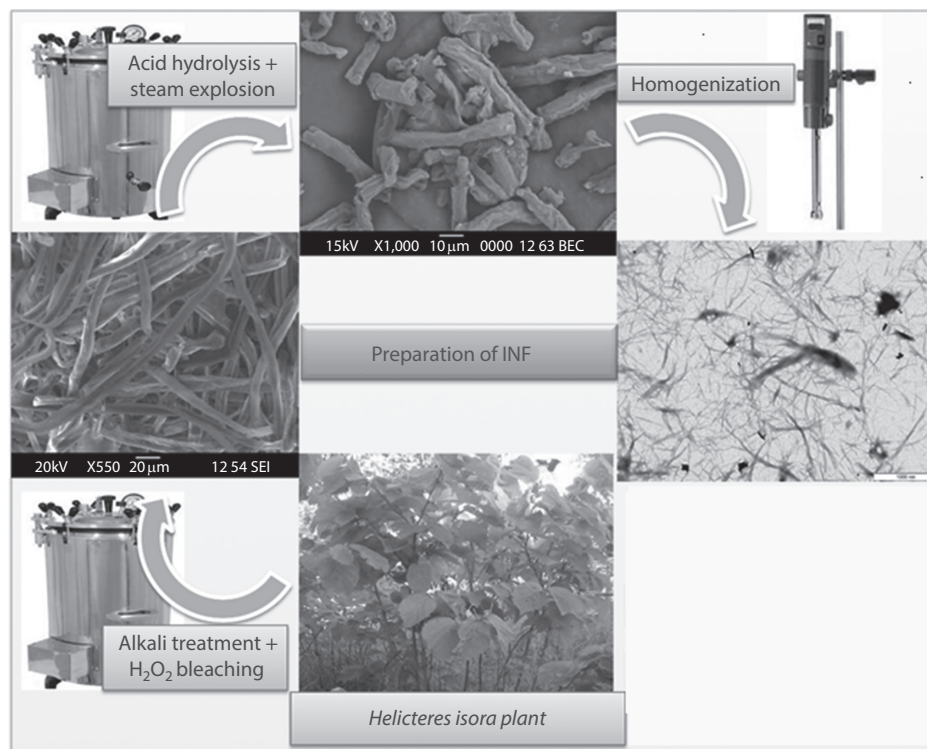


Figure 1 Procedure for the preparation of INF from *Helicteres isora* bark.

was used to examine the size of INF. A drop of a diluted suspension (1 wt%) was deposited on the surface of a clean copper grid coated with a thin carbon film. The sample was dried at ambient temperature before TEM analysis and the measurement was carried out with an accelerating voltage of 80 kV. Fourier transform infrared spectroscopy (FTIR) spectrum of INF was recorded using a Shimadzu IR-470 IR spectrophotometer. The FTIR spectrum of each sample was obtained in the wavelength range of 400–4000 cm^{-1} , with a resolution of 2 cm^{-1} and a total of 15 scans for each sample. X-ray diffraction technique was employed to analyze the crystallinity of INF after different chemical treatments. X-ray equatorial diffraction patterns of raw, alkali-treated, H_2O_2 -bleached and acid-treated fibrils were obtained with an X-ray diffractometer (JEOL diffractometer, Model JDX 8P) using CuK radiation ($\lambda = 0.1539 \text{ nm}$) at operating voltage and current of 40 kV and 20 mA respectively. X-ray diffractograms were obtained at room temperature within a 2θ range from 5 to 80° at a scan rate of $2^\circ/\text{min}$. Crystallinity index (I_{cr}) of the material was determined by Segal method, as shown in Equation 1 [51].

$$I_{cr} (\%) = \frac{I_{002} - I_{am}}{I_{002}} \quad (1)$$

Where I_{cr} expresses the relative degree of crystallinity, I_{002} is the maximum intensity of (0 0 2) lattice diffraction at $2\theta = 22^\circ$, and I_{am} is the intensity of diffraction at $2\theta = 16^\circ$; I_{002} represents both crystalline and amorphous regions, while I_{am} represents only the amorphous part. Thermal stability of INF fibers was determined using a thermogravimetric analyzer (TGA Q5000). All measurements were performed under nitrogen atmosphere with a gas flow of 10 mL/min by heating the material from room temperature to 700°C at a heating rate of $10^\circ\text{C}/\text{min}$.

2.3.2 PBS-INF Composites

The dispersion state of INF within the resulting PBS-INF composites was investigated using TEM. For this, ultra-thin films of each type of composite (thickness

of 50 nm) were obtained by ultra-microtome cutting. Static tensile properties (i.e., modulus, strength and toughness) were measured at room temperature ($\sim 25^\circ\text{C}$) and atmospheric conditions (relative humidity: $\sim 50 \pm 5\%$) using an Instron Universal Testing Machine (Model# 5985) equipped with a 1 kN load cell, with tests being carried out at crosshead speed of 10 mm/min in accordance with ISO 20753 A₁₂ and five identical specimens being tested for each formulation. Flexural tests were conducted using a three-point bending fixture on an Instron Universal Testing Machine (Model# 5985) equipped with a 1kN load cell, with tests being carried out at a test speed of 2 mm/min up to 16% bending in accordance with ISO 178. Span-to-depth ratio was 16, with average values of flexural strength and modulus of each composite calculated using five specimens each.

3 RESULTS AND DISCUSSIONS

3.1 Isora Fiber

3.1.1 Compositional Analysis

The chemical composition of isora fiber after different chemical treatments is summarized in Table 1. As the results illustrate, isora fiber is an attractive source of nanocellulose due to its higher cellulose content compared to other commonly used natural fibers such as banana (*Musa spp.*) (54–64.4%) [41, 52], sugarcane (*Saccharum officinarum*) bagasse (44.9–45%) [54], bamboo (*Bambusa spp.*) (41.8–54.0%) [55], and coconut (*Cocos nucifera*) husk (32.5–45.9%) [56]. The results also reveal that chemical treatments removed almost all the hemicellulose (0.6%) and lignin (1.4%) from the fibers, accompanied with a drastic increase in cellulose content from 72% to 94%. The sum of percentage content of cellulose, hemicellulose and lignin corresponds to the total dry matter, indicating the presence of other components like pectin, wax, and moisture.

When raw fiber was subjected to alkali treatment followed by steam explosion, hemicellulose was undergoing hydrolysis, while lignin was going through depolymerization, giving rise to sugars and phenolic

Table 1 Chemical composition of fibers at each stage of treatment.

Fiber	Cellulose (%) (TAPPI T19 m-54)	Hemicellulose (%) (TAPPI T19 m-54)	Lignin (%) (TAPPI-T222 om-88)
Raw	72.0 ± 3.1	3.1 ± 2.4	21.2 ± 0.9
Alkali treated	76.3 ± 2.9	1.8 ± 3.1	15.5 ± 2.4
H_2O_2 bleached	86.1 ± 1.8	1.1 ± 0.9	2.1 ± 1.4
Acid hydrolysis	94.3 ± 3.3	0.6 ± 2.3	1.4 ± 3.2

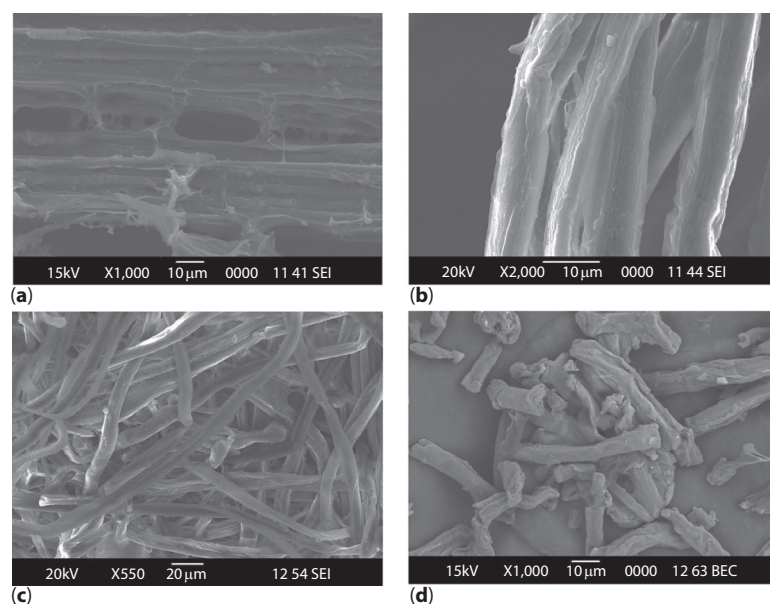


Figure 2 SEM images of (a) Untreated fiber (b) Alkali-treated isora fiber (c) Bleached fiber (d) Acid - hydrolyzed fiber.

resin compounds that are partially soluble in water [57]. Generally, steam explosion ends up in a chemical reaction of glycosidic bonds within hemicellulose, resulting in the cleavage of hemicelluloses-lignin bonds [58]. High solubility of lignin and hemicelluloses was due to the cleavage of the ether linkages between lignin and hemicellulose by alkali treatment [59]. Yield of INF with respect to the initial amount of dried isora fibers was 58%, higher than the nanofiber obtained from isora fiber by chlorine-based bleaching [48]. Hence, it can be used as a potential source for scaling up the production of cellulose nanofibrils.

3.1.2 Morphology

Scanning electron microscopy (SEM) images of the isora fiber at different processing stages are shown in Figure 2. Figure 2a shows the surface of raw fiber [60]. After alkali treatment, due to the partial removal of materials such as lignin, hemicellulose, pectin, wax and other impurities, the fiber surface becomes smooth, as shown in Figure 2b. The H_2O_2 bleaching treatment caused defibrillation of fiber bundles by removal of binding material and reduction in fiber diameter (Figure 2c) [60]. Further decrease in the diameter of fibers was observed post acid treatment (Figure 2d) [34]. After homogenization these acid-treated fibers result in further defibrillation yielding INF.

3.1.3 FTIR Analysis

The FTIR spectra of isora fiber at different stages are shown in Figure 3. As can be seen in Figure 3, all

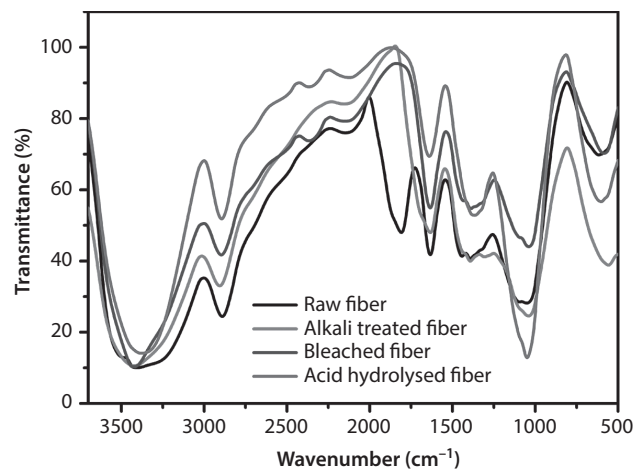


Figure 3 FTIR spectra of raw fiber, alkali treated, H_2O_2 bleached and acid hydrolysed isora fibers.

prominent bands corresponding to cellulose, including 3341, 2901, 1429, 1161, 1110 and 897 cm^{-1} , are present in all the spectra [61–63]. However, for raw fibers, additional bands at 1731 cm^{-1} correspond to acetyl and uronic ester groups of hemicelluloses and the ester linkage of carboxylic group of the ferulic and p-coumaric acids of lignin. The peak at 1509 cm^{-1} originating from the aromatic $C=C$ stretching was also present [64]. As the fibers are subjected to alkali treatment and H_2O_2 bleaching, intensities of all these peaks showed a reduction, indicating the partial removal of lignin and hemicellulose [65–67]. As expected, the data presented in Table 1 shows that hemicellulose and lignin are not entirely removed by these chemical treatments and a

small amount is always retained even after various chemical treatments [25, 68].

3.1.4 X-Ray Diffraction Analysis

Chemical treatments that are capable of removing noncellulosic biomass can affect the crystallinity of cellulose. Figure 4 shows the XRD patterns of raw fiber and of fibers at different chemical treatment stages. Raw fiber shows a strong crystalline peak at 2θ values: 22.6° for (2 0 0) plane, and a broad peak at 16° for (1 0 1) plane. As can be seen from Figure 4, all the samples exhibited a sharp diffraction peak at 22° , which is characteristic of cellulose I structure [69]. In the case of nanofibers, the diffractogram demonstrates a considerable increase in the sharpness of edge. Moreover, for INF, the peak at 16° became broader with an observable shoulder, indicating the highly enriched structure of cellulose.

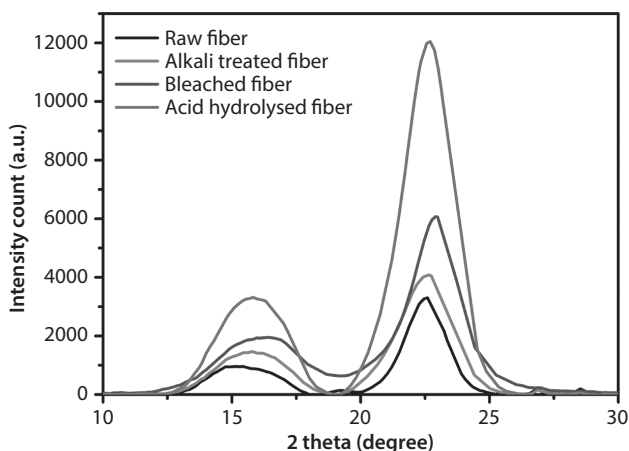


Figure 4 XRD spectra of raw fiber, alkali treated, H_2O_2 bleached and acid hydrolysed isora fibers.

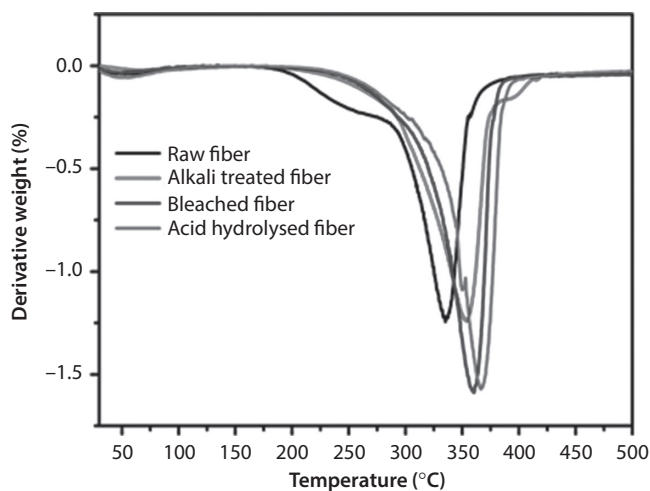
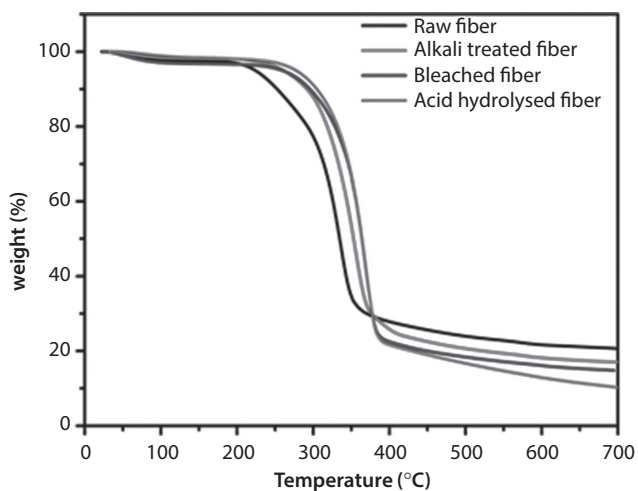


Figure 5 TG curves of raw, alkali treated, H_2O_2 bleached and acid hydrolyzed isora fiber.

The I_{cr} was calculated according to Segal’s method, which provides a quantitative measure of the crystallinity in powders [51]. A higher crystallinity index for chemically treated isora fibers in comparison to the raw fibers can be attributed to the efficient removal of hemicellulose and lignin from the amorphous regions, and the enrichment of cellulose content in isora fibers due to alkali and H_2O_2 bleaching treatments (Table 2). Therefore, INF obtained from the combined application of chemical treatments and high pressure homogenization treatment in the present work can be highly effective in achieving better reinforcement in composite materials [25].

3.1.5 Thermogravimetric Analysis

Raw, alkali-treated, H_2O_2 -bleached, and homogenized isora fiber samples were thermogravimetrically analyzed to compare the degradation characteristics at different stages of preparation (Figure 5). Initial weight loss observed in the temperature region of $60\text{--}110^\circ\text{C}$ was due to vaporization and removal of bound water in the cellulose samples. Weight reduction beginning at 220°C was due to the degradation of hemicellulose, which has lower thermal stability than lignin and cellulose [70]. Massive degradation observed in the temperature region from 250 to 450°C

Table 2 Crystallinity Index of the fibers

Fiber	Crystallinity index (I_{cr})
Raw	34.11
Alkali treated	49.26
H_2O_2 bleached	77.25
Acid hydrolysis	88.68

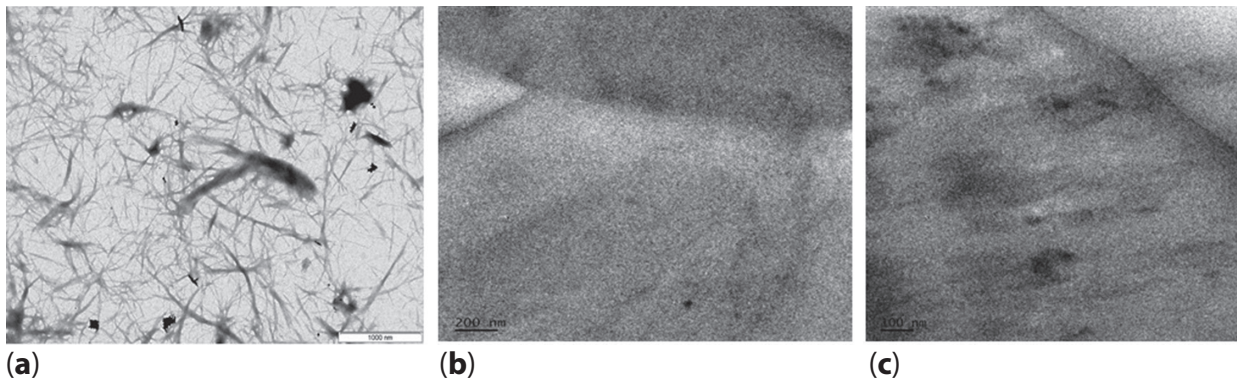


Figure 6 TEM image of (a) INF, (b) PBS-0.5 INF and (c) PBS-1.5 INF.

was due to the degradation of lignin and cellulose components.

From the DTG curve it is clear that various chemical treatments led to an enhancement in thermal stability of the isora fiber. Presence of hemicellulose, pectin, and lignin may expedite thermal degradation of isora fibers by providing more active sites for initiating such degradation. The different chemical treatments led to the removal of these components, thereby improving its thermal stability. At 700 °C, the lowest char yield was obtained for the acid-treated cellulose due to the removal of noncellulosic components in the fiber.

3.2 PBS-INF Composites

3.2.1 Morphology

The INF and composites were imaged using TEM as well. Figure 6a shows the INF fiber before mixing with PBS. The TEM images in Figure 6b and 6c show the dispersion state of INF at 0.5 and 1.5 phr in the corresponding PBS-INF composites. It was difficult to obtain uniformly dispersed nanocellulose from natural plant fibers since the nanophase has a strong tendency to form larger structures via aggregation and agglomeration [71].

3.2.2 Mechanical Properties

Figure 7 shows stress-strain curves of pure PBS and PBS-INF nanocomposites, indicating the occurrence of an initial yielding, followed by a drop in stress. This was due to a reduction in the cross-sectional area on account of necking and breakage of the secondary bonds (i.e., van der Waals and hydrophobic interactions) that connected the crystal structure, leading to the occurrence of the slip between polymer chains [72]. This was followed by severe necking and strain hardening, as indicated by the gradual rise of the stress-strain curve. It is also interesting to note that the

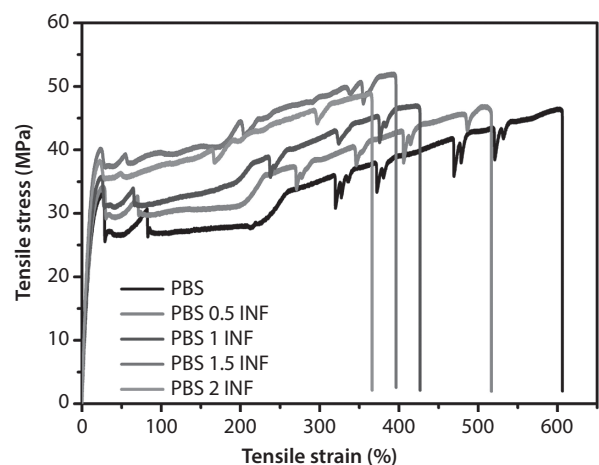


Figure 7 Tensile stress-strain curves of PBS and PBS-INF nanocomposites.

failure stress was observed to be higher than the initial yield stress usually accompanied by strain-induced crystallization, which would have aligned the crystallites in the direction of strain [12]. All specimens showed a tendency to follow ductile fracture mode, as evidenced from the stress-strain curves. Ductility was gauged by strain-at-break and toughness. Lin *et al.* observed that addition of 2 wt% cellulose nanowiskers improved the tensile strength from 26.2 to 29 MPa [46].

Toughness, which is defined as energy-to-fracture per unit volume of the specimen, is obtained by integrating area under the stress-strain curve. Toughness of PBS-INF nanocomposites showed a significant decrease when compared to pure PBS (Figure 8). This decrease in toughness may be attributed to the fact that INF particles acted as stress concentrators [73]. Area up to the yield point in the stress-strain curve is termed “modulus of resilience.” Modulus of resilience of the PBS-INF composites (Figure 8) showed an increase up to the loading level of 1.5 phr INF

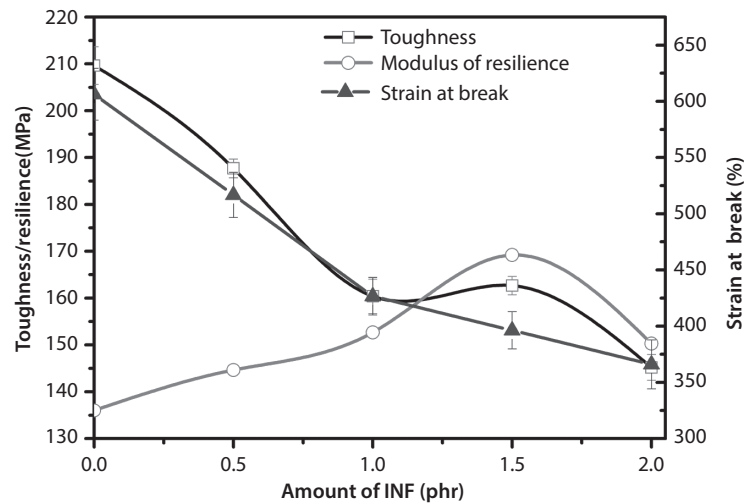


Figure 8 Toughness, modulus of resilience and strain at break of PBS and PBS-INF nanocomposites.

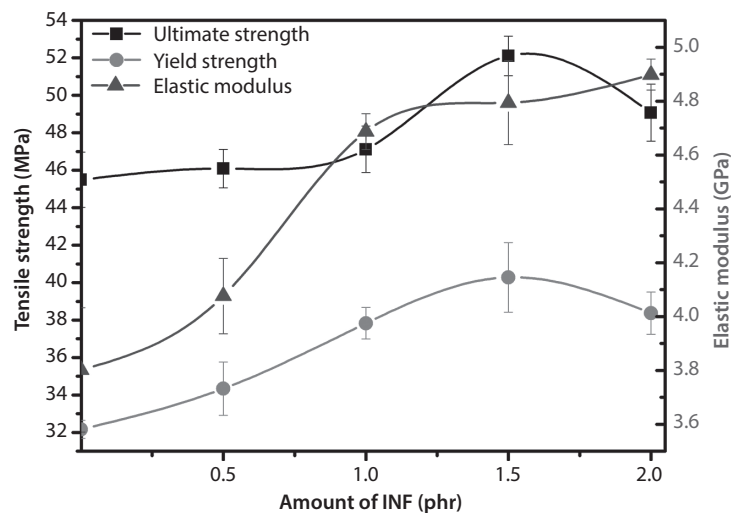


Figure 9 Ultimate strength, yield strength and elastic modulus of PBS and PBS-INF nanocomposites.

due to interfacial interaction between the fibers and matrix [74]. Strain-at-break (%) showed a decrease with increase in INF content (Figure 8). For example, strain-at-break was observed to decrease from 606% (neat PBS) to 368% upon addition of 2 phr INF. The decreased deformability of PBS matrix was due to the enhanced restriction offered by INF.

Young's modulus of PBS-INF nanocomposites increased with INF content (Figure 9). Modulus was observed to become enhanced from 3.8 GPa (neat PBS) to 4.9 GPa upon addition of 2 phr INF, an increase of nearly 29%. This increment in modulus was due to the enhanced restriction of polymer chains offered by INF. In fact, the INF is able to form a network in the PBS matrix by hydrogen bonding interaction which can suppress the mobility of the PBS chains, leading to an increase in stiffness and strength and decrease

in toughness and elongation at break. In this study, enhancement in ultimate tensile strength and yield strength were observed for nanocomposites up to a loading level of 1.5% INF (Figure 9). Addition of 1.5 phr INF was observed to lead to the enhancement of ultimate tensile strength by 14% and of yield strength by 25.2% compared to corresponding values for neat PBS. However, beyond 1.5% INF loading, both strength parameters showed a decline. This could be due to possible agglomeration of INF reducing the effective interfacial area, thereby leading to a compromise on tensile strength. Lin *et al.* have observed a similar phenomenon for cellulose whisker (CW)-reinforced PBS composites. They reported an enhancement in tensile strength from 26 MPa (for neat PBS) to 29 MPa upon loading of 2 wt% of CW; although further increase in CW content led to a decline in tensile strength [46].

3.2.3 Theoretical Model Predictions: Comparison of the Mechanical Properties

To gain a better understanding of the interactions between PBS and INF, tensile strength and Young's modulus data were analyzed by comparing them with various prediction models/theories.

3.2.3.1 Relative Tensile Strength (RTS)

Relative tensile strength is the ratio of tensile strength of the composite to the tensile strength of pure matrix. Four theoretical models were used to predict the RTS of PBS-INF composites. These are described below in detail.

- a. Rule of mixture (ROM) and Inverse rule of mixtures (IROM):

ROM and IROM equations (Equations 2 and 3) represent the simplest model that can be used to predict the tensile strength of a composite. ROM equation (Equation 2) is used to predict the upper limit of tensile strength while IROM equation (Equation 3) is used to predict the lower limit of tensile strength [75].

$$\sigma_C = \sigma_{INF} \phi_{INF} + \sigma_{PBS} \phi_{PBS} \quad (2)$$

$$\sigma_C = \frac{\sigma_{INF} \sigma_{PBS}}{\sigma_{INF} \phi_{PBS} + \sigma_{PBS} \phi_{INF}} \quad (3)$$

Here, σ_C , σ_{INF} and σ_{PBS} refer to tensile strength of the composite, isora fiber and neat PBS respectively, while ϕ_{INF} and ϕ_{PBS} refer to volume fraction of INF and PBS respectively in the nanocomposite.

- b. Nicolais-Narkis model:

This model assumes no adhesion between the filler and matrix. Based on this assumption, RTS is calculated using Equation 4 given below.

$$RTS = \frac{\sigma_C}{\sigma_{PBS}} = 1 - 1.20 \phi_{INF}^{2/3} \quad (4)$$

- c. Halpin-Tsai model:

In this model, perfect interaction is assumed between the filler and matrix. Based on this assumption, RTS is calculated using Equation 5, where ξ is calculated using Equation 6.

$$RTS = \frac{\sigma_C}{\sigma_{PBS}} = \frac{1 + \xi \eta_T \phi_{INF}}{1 - \eta_T \phi_{INF}} \quad (5)$$

$$\xi = \frac{2l}{3d} \quad (6)$$

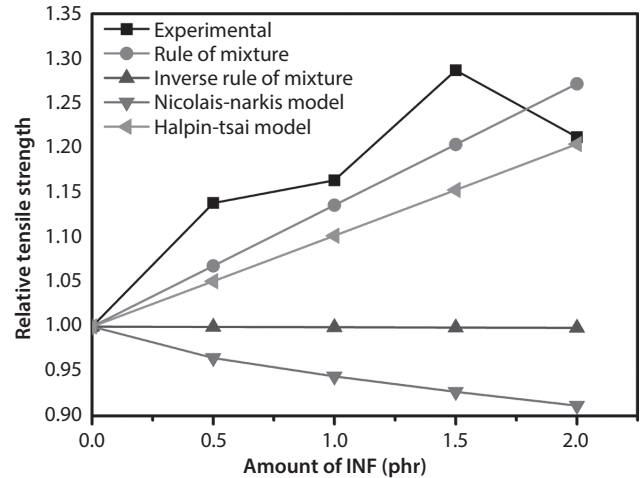


Figure 10 Comparison of experimental RTS values of PBS-INF composites with values obtained from theoretical models.

$$\eta_T = \frac{(E_{INF} / E_{PBS}) - 1}{(E_{INF} / E_{PBS}) + 2} \quad (7)$$

Here, l and d refer to the average length and diameter of INF fibers and E_{INF} and E_{PBS} refer to the Young's modulus of filler and PBS respectively.

Figure 10 compares the experimentally obtained values of RTS with theoretically obtained RTS values based on the four models mentioned above for various INF loadings. As can be seen, experimental results are observed to match better, relatively, with theoretical values obtained using ROM and Halpin-Tsai models compared to Nicolais-Narkis and Inverse ROM models. Percentage deviation of experimentally obtained RTS values from theoretically obtained value is very large in the case of Nicolais-Narkis and inverse ROM models compared to that from Halpin-Tsai and ROM models. This suggests the existence of some type of interaction between INF and PBS.

3.2.3.2 Relative Young's Modulus (RYM)

Relative Young's modulus is the ratio of Young's modulus of the composite to the Young's modulus of pure matrix. It can also be obtained using three different models as given below.

- a. ROM-IROM model:

ROM and IROM equations (Equations 8 and 9) represent the simplest model that can be used to predict the elastic modulus of a composite. ROM equation (Equation 8) is used to predict the upper limit of elastic modulus while IROM

equation (Equation 9) is used to predict the lower limit of elastic modulus [76].

$$E_C = E_{INF} \phi_{INF} + E_{PBS} \phi_{PBS} \tag{8}$$

$$E_C = \frac{E_{INF} E_{PBS}}{E_{INF} \phi_{PBS} + E_{PBS} \phi_{INF}} \tag{9}$$

b. Halpin-Tsai model:

This model [77] predicts the elastic constants of composite materials as a function of aspect ratio of the filler, when the constituent properties and volume fractions of the two phases (matrix and reinforcement) are known. Elastic modulus (E_C) of a randomly oriented short fiber composite is given by Equation 10, where E_L and E_T are longitudinal and traverse moduli respectively, and are calculated using Equations 11 and 12.

$$E_C = \frac{3}{8} E_L + \frac{5}{8} E_T \tag{10}$$

$$E_L = E_{PBS} \left[\frac{1 + (2l/d) \eta_L \phi_{INF}}{1 - \eta_L \phi_{INF}} \right] \tag{11}$$

$$E_T = E_{PBS} \left[\frac{1 + 2\eta_T \phi_{INF}}{1 - \eta_T \phi_{INF}} \right] \tag{12}$$

Constants η_L and η_T are calculated using Equations 13 and 7, while (l/d) represents the aspect ratio of enforcement.

$$\eta_L = \frac{(E_{INF} / E_{PBS}) - 1}{(E_{INF} / E_{PBS}) + (2l/d)} \tag{13}$$

Figure 11 shows the variation in relative Young’s modulus (RYM) with change in volume fraction of filler in the composites. Experimentally obtained RYM values were compared with theoretical RYM values obtained using ROM, IROM and Halpin-Tsai models. RYM value showed a progressive increase with INF content due to the stiffening effect of INF. Halpin-Tsai model assumes the existence of perfect adhesion between the filler and its matrix, and experimentally obtained RYM results in this study were observed to be closer to the Halpin-Tsai model, as was also found for the RTS values [78]. While the Halpin-Tsai model supposes a perfect interface between matrix and fiber, it does not account for fiber-fiber interactions which can take place in high loading cellulose composite/nanocomposites (i.e., percolated networks).

Young’s modulus of cellulose fibers can vary according to the source of cellulose and based on fiber dimensions. Young’s modulus of 40–60 GPa is usually found for natural bast fibers like flax and hemp, while it potentially increases up to 80 GPa for single cells and is in the range of 100–140 GPa for nanofibrils and nanowhiskers [79].

Flexural strength of a material is its ability to resist deformation under load. Figure 12 shows the flexural strength and modulus of PBS and PBS-INF nanocomposites. Flexural properties of INF-reinforced PBS nanocomposites were observed to show a similar trend as tensile properties. Flexural strength of PBS-INF nanocomposites was observed to become enhanced upon the addition of INF up to 1.5 phr; for example, flexural strength showed an increased

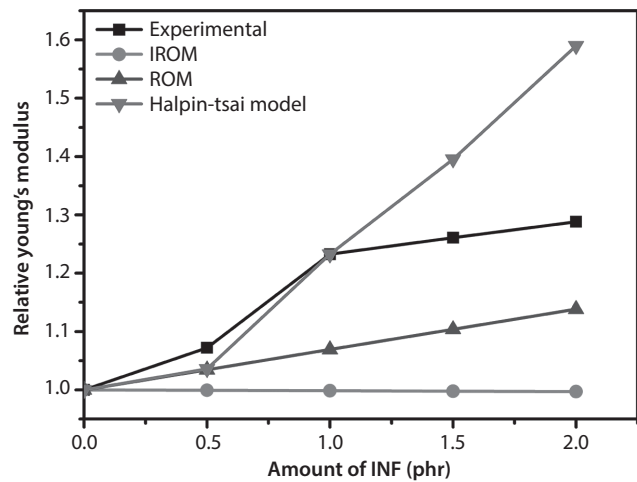


Figure 11 Comparison of experimentally obtained RYM values of PBS-INF composites with values of the theoretical models.

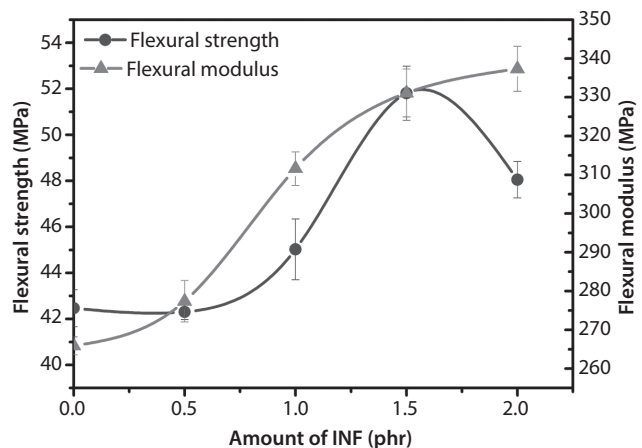


Figure 12 Flexural strength and flexural modulus of PBS and PBS-INF nanocomposites.

from 42.5 MPa for neat PBS to 52 MPa upon addition of 1.5 phr INF, showing an increase of 22%. This improvement in flexural strength could be due to the formation of mechanical interlocks between INF and PBS, giving the PBS matrix ability to withstand the bending force [16]. Moreover, collapse of the fiber-matrix interface upon bending is expected to allow better contact between the matrix and reinforced fibers [16]. This physical interaction would have allowed the applied load to be transferred to the fibers via mechanical shearing at the fiber-matrix interface. Beyond 1.5 phr of INF loading, flexural strength was observed to decline, which may be due to the reduced interaction between PBS and INF on account of agglomeration of INF. The stiffening effect of INF led to improvement in the flexural modulus of PBS-INF nanocomposites. In fact, similar to tensile modulus, flexural moduli also showed an increase with INF content due to the enhanced restriction of polymer chains offered by INF.

4 CONCLUSIONS

In this study, isora nanofibers were extracted from *Helicteres isora* by using combined thermal-chemical-mechanical treatments. Morphology, structural analysis and thermal stability of cellulose fiber were analyzed at each step using scanning electron microscopy (SEM), transmission electron microscopy (TEM), Fourier transform infrared (FTIR) spectroscopy, X-ray diffraction analysis (XRD) and thermogravimetric analysis (TGA). The FTIR results indicated that chemical treatments progressively removed noncellulosic constituents and analysis of XRD results revealed an increase in the crystallinity of fiber with successive treatments. A and DTG results showed that isora nanofiber possessed higher thermal stability. Sustainable and biodegradable nanocomposites were prepared using PBS and INF. All specimens tended to follow ductile fracture mode, as evidenced from the stress-strain curves. Addition of INF was observed to lead to an increase in resilience, tensile and flexural moduli of PBS-INF nanocomposites, but was accompanied with a decline in toughness and strain-at-break of the nanocomposites. INF showed a promising reinforcing ability by enhancing both tensile and flexural strengths up to 1.5 phr INF loading. However, beyond this level of loading, both the strength parameters were observed to decline due to possible agglomeration of INF. Thus, the optimum INF loading for enhanced (tensile and flexural) stiffness and strength properties was found to be 1.5 phr. Theoretically predicted tensile strength and Young's modulus were found to increase with INF content; however, a mismatch was observed

to exist between theoretically predicted and experimentally observed results due to reasons discussed previously.

ACKNOWLEDGMENTS

The authors are grateful to Kimberly Ivey for her assistance in conducting TGA tests. This work was partially supported by the USDA National Institute of Food and Agriculture, AFRI project [2016-67021-25016]. The first author would like to acknowledge the fellowship support of University Grants Commission, India.

REFERENCES

1. S.-H. Lee and S. Wang, Biodegradable polymers/bamboo fiber biocomposite with bio-based coupling agent. *Compos. Part A Appl. Sci. Manuf.* **37**, 80–91 (2006). doi:10.1016/j.compositesa.2005.04.015.
2. Y.J. Phua, W.S. Chow, and Z.A. Mohd Ishak, Organomodification of montmorillonite and its effects on the properties of poly(butylene succinate) nanocomposites. *Polym. Eng. Sci.* **53**, 1947–1957 (2013). doi:10.1002/pen.23460.
3. Y.J. Phua, N.S. Lau, K. Sudesh, W.S. Chow, and Z.A. Mohd Ishak, Biodegradability studies of poly(butylene succinate)/organo-montmorillonite nanocomposites under controlled compost soil conditions: Effects of clay loading and compatibiliser. *Polym. Degrad. Stab.* **97**, 1345–1354 (2012). doi:10.1016/j.polymdegradstab.2012.05.024.
4. M.N. Satheesh Kumar, A.K. Mohanty, L. Erickson, and M. Misra, Lignin and its applications with polymers. *J. Biobased Mater. Bioenergy.* **3**, 1–24 (2009). doi:10.1166/jbmb.2009.1001.
5. S. Sahoo, M. Misra, and A.K. Mohanty, Enhanced properties of lignin-based biodegradable polymer composites using injection moulding process. *Compos. Part A Appl. Sci. Manuf.* **42**, 1710–1718 (2011). doi:10.1016/j.compositesa.2011.07.025.
6. K. Abe, S. Iwamoto, and H. Yano, Obtaining cellulose nanofibres with a uniform width of 15 nm from wood. *Biomacromolecules.* **8**, 3276–3278, (2007).
7. G. Siqueira, H. Abdillahi, J. Bras, and A. Dufresne, High reinforcing capability cellulose nanocrystals extracted from *Syngonanthus nitens* (Capim Dourado). *Cellulose.* **17**, 289–298 (2009). doi:10.1007/s10570-009-9384-z.
8. N. Soykeabkaew, P. Supaphol, and R. Rujiravanit, Preparation and characterization of jute- and flax-reinforced starch-based composite foams. *Carbohydr. Polym.* **58**, 53–63 (2004). doi:10.1016/j.carbpol.2004.06.037.
9. T. Ohkita and S.-H. Lee, Crystallization behavior of poly(butylene succinate)/corn starch biodegradable composite. *J. Appl. Polym. Sci.* **97**, 1107–1114 (2005). doi:10.1002/app.21741.
10. L. Bao, Y. Chen, W. Zhou, Y. Wu, and Y. Huang, Bamboo fibers @ poly(ethylene glycol)-reinforced poly(butylene succinate) biocomposites. *J. Appl. Polym. Sci.* **122**, 2456–2466 (2011). doi:10.1002/app.

11. L. Liu, J. Yu, L. Cheng, and X. Yang, Biodegradability of poly(butylene succinate) (PBS) composite reinforced with jute fibre. *Polym. Degrad. Stab.* **94**, 90–94 (2009). doi:10.1016/j.polymdegradstab.2008.10.013.
12. U.S. Ishiaku, O.A. Khondker, S. Baba, A. Nakai, and H. Hamada, Processing and characterization of short-fiber reinforced jute/poly butylene succinate biodegradable composites: The effect of weld-line. *J. Polym. Environ.* **13**, 151–157 (2005). doi:10.1007/s10924-005-2946-8.
13. T. Bin, J. Qu, L. Liu, Y. Feng, S. Hu, and X. Yin, Non-isothermal crystallization kinetics and dynamic mechanical thermal properties of poly(butylene succinate) composites reinforced with cotton stalk bast fibers. *Thermochim. Acta.* **525**, 141–149 (2011). doi:10.1016/j.tca.2011.08.003.
14. Y.-H. Feng, D.-W. Zhang, J.-P. Qu, H.-Z. He, and B.-P. Xu, Rheological properties of sisal fiber/poly(butylene succinate) composites. *Polym. Test.* **30**, 124–130 (2011). doi:10.1016/j.polymertesting.2010.11.004.
15. T.H. Nam, S. Ogihara, N.H. Tung, and S. Kobayashi, Effect of alkali treatment on interfacial and mechanical properties of coir fiber reinforced poly(butylene succinate) biodegradable composites. *Compos. Part B Eng.* **42**, 1648–1656 (2011). doi:10.1016/j.compositesb.2011.04.001.
16. M.Z.A. Thirmizir, Z.A.M. Ishak, R.M. Taib, S. Rahim, and S.M. Jani, Kenaf-bast-fiber-filled biodegradable poly(butylene succinate) composites: Effects of fiber loading, fiber length, and maleated poly(butylene succinate) on the flexural and impact properties. *J. Appl. Polym. Sci.* **122**, 3055–3063 (2011). doi:10.1002/app.
17. C.-F. Kuan, C.-C.M. Ma, H.-C. Kuan, H.-L. Wu, and Y.-M. Liao, Preparation and characterization of the novel water-crosslinked cellulose reinforced poly(butylene succinate) composites. *Compos. Sci. Technol.* **66**, 2231–2241 (2006). doi:10.1016/j.compscitech.2005.12.011.
18. V.M. Correlo, L.F. Boesel, M. Bhattacharya, J.F. Mano, N.M. Neves, and R.L. Reis, Hydroxyapatite reinforced chitosan and polyester blends for biomedical applications. *Macromol. Mater. Eng.* **290**, 1157–1165 (2005). doi:10.1002/mame.200500163.
19. S.O. Han, S.M. Lee, W.H. Park, and D. Cho, Mechanical and thermal properties of waste silk fiber-reinforced poly(butylene succinate) biocomposites. *J. Appl. Polym. Sci.* **100**, 4972–4980 (2006). doi:10.1002/app.23300.
20. M.W. Lee, S.O. Han, and Y.B. Seo, Red algae fibre/poly(butylene succinate) biocomposites: The effect of fibre content on their mechanical and thermal properties. *Compos. Sci. Technol.* **68**, 1266–1272 (2008). doi:10.1016/j.compscitech.2007.12.016.
21. E.D.M. Teixeira, T.J. Bondancia, K.B.R. Teodoro, A.C. Corrêa, J.M. Marconcini, and L.H.C. Mattoso, Sugarcane bagasse whiskers: Extraction and characterizations. *Ind. Crops Prod.* **33**, 63–66 (2011). doi:10.1016/j.indcrop.2010.08.009.
22. S.M. Costa, P.G. Mazzola, J.C.A.R. Silva, R. Pahl, A. Pessoa, and S.A. Costa, Use of sugar cane straw as a source of cellulose for textile fiber production. *Ind. Crops Prod.* **42**, 189–194 (2013). doi:10.1016/j.indcrop.2012.05.028.
23. A. Mandal and D. Chakrabarty, Isolation of nanocellulose from waste sugarcane bagasse (SCB) and its characterization. *Carbohydr. Polym.* **86**, 1291–1299 (2011). doi:10.1016/j.carbpol.2011.06.030.
24. M. Ghaderi, M. Mousavi, H. Yousefi, and M. Labbafi, All-cellulose nanocomposite film made from bagasse cellulose nanofibers for food packaging application. *Carbohydr. Polym.* **104**, 59–65 (2014). doi:10.1016/j.carbpol.2014.01.013.
25. M. Li, L.J. Wang, D. Li, Y.L. Cheng, and B. Adhikari, Preparation and characterization of cellulose nanofibers from de-pectinated sugar beet pulp. *Carbohydr. Polym.* **102**, 136–143 (2014). doi:10.1016/j.carbpol.2013.11.021.
26. M.R. Vignon, A. Dufresne, and J. Cavaille, Mechanical behavior of sheets prepared from sugar beet cellulose microfibrils. *J. Appl. Polym. Sci.* **64**, 1185–1194 (1997).
27. E. Dinand, H. Chanzy, and R.M. Vignon, Suspensions of cellulose microfibrils from sugar beet pulp. *Food Hydrocoll.* **13**, 275–283 (1999). doi:10.1016/S0268-005X(98)00084-8.
28. D. Chen, D. Lawton, M.R. Thompson, and Q. Liu, Biocomposites reinforced with cellulose nanocrystals derived from potato peel waste. *Carbohydr. Polym.* **90**, 709–716 (2012). doi:10.1016/j.carbpol.2012.06.002.
29. S. Arun, K.A.A. Kumar, and M.S. Sreekala, Fully biodegradable potato starch composites: Effect of macro and nano fiber reinforcement on mechanical, thermal and water-sorption characteristics. *Int. J. Plast. Technol.* **16**, 50–66 (2012). doi:10.1007/s12588-012-9026-4.
30. C. Rondeau-Mouro, B. Bouchet, B. Pontoire, P. Robert, J. Mazoyer, and A. Buléon, Structural features and potential texturing properties of lemon and maize cellulose microfibrils. *Carbohydr. Polym.* **53**, 241–252 (2003). doi:10.1016/S0144-8617(03)00069-9.
31. D.M. Nascimento, J.S. Almeida, A.F. Dias, M.C.B. Figueirêdo, J.P.S. Morais, J.P.A. Feitosa, et al., A novel green approach for the preparation of cellulose nanowhiskers from white coir. *Carbohydr. Polym.* **110**, 456–463 (2014). doi:10.1016/j.carbpol.2014.04.053.
32. F.Z. Arrakhiz, M. Malha, R. Bouhfid, K. Benmoussa, and A. Qaiss, Tensile, flexural and torsional properties of chemically treated alfa, coir and bagasse reinforced polypropylene. *Compos. Part B Eng.* **47**, 35–41 (2013). doi:10.1016/j.compositesb.2012.10.046.
33. D. Verma, P.C. Gope, A. Shandilya, A. Gupta, and M.K. Maheshwari, Coir fibre reinforcement and application in polymer composites: A review. *J. Mater. Environ. Sci.* **4**, 263–276 (2013).
34. E. Abraham, B. Deepa, L.A. Pothan, J. Cintil, S. Thomas, M.J. John, et al., Environmental friendly method for the extraction of coir fibre and isolation of nanofibre. *Carbohydr. Polym.* **92**, 1477–1483 (2013). doi:10.1016/j.carbpol.2012.10.056.
35. M.F. Rosa, E.S. Medeiros, J.A. Malmonge, K.S. Gregorski, D.F. Wood, L.H.C. Mattoso, et al., Cellulose nanowhiskers from coconut husk fibers: Effect of preparation conditions on their thermal and morphological behavior. *Carbohydr. Polym.* **81**, 83–92 (2010). doi:10.1016/j.carbpol.2010.01.059.
36. F. Fahma, S. Iwamoto, N. Hori, T. Iwata, and A. Takemura, Effect of pre-acid-hydrolysis treatment on morphology and properties of cellulose nanowhiskers from

- coconut husk. *Cellulose*. **18**, 443–450 (2010). doi:10.1007/s10570-010-9480-0.
37. R. Zuluaga, J.L. Putaux, J. Cruz, J. Vélez, I. Mondragon, and P. Gañán, Cellulose microfibrils from banana rachis: Effect of alkaline treatments on structural and morphological features. *Carbohydr. Polym.* **76**, 51–59 (2009). doi:10.1016/j.carbpol.2008.09.024.
38. M. Boopalan, M. Niranjanaa, and M.J. Umopathy, Study on the mechanical properties and thermal properties of jute and banana fiber reinforced epoxy hybrid composites. *Compos. Part B Eng.* **51**, 54–57 (2013). doi:10.1016/j.compositesb.2013.02.033.
39. S. Elanthikkal, U. Gopalakrishnapanicker, S. Varghese, and J.T. Guthrie, Cellulose microfibrils produced from banana plant wastes: Isolation and characterization. *Carbohydr. Polym.* **80**, 852–859 (2010). doi:10.1016/j.carbpol.2009.12.043.
40. B.M. Cherian, L.A. Pothan, T. Nguyen-Chung, G. Mennig, M. Kottaisamy, and S. Thomas, A novel method for the synthesis of cellulose nanofibril whiskers from banana fibers and characterization. *J. Agric. Food Chem.* **56**, 5617–5627 (2008).
41. B. Deepa, E. Abraham, B.M. Cherian, A. Bismarck, J.J. Blaker, L.A. Pothan, et al., Structure, morphology and thermal characteristics of banana nano fibers obtained by steam explosion. *Bioresour. Technol.* **102**, 1988–1997 (2011). doi:10.1016/j.biortech.2010.09.030.
42. S.S.-Y. Lee, D.J. Mohan, I.-A. Kang, G. Doh, S.S.-Y. Lee, and S.O. Han, Nanocellulose reinforced PVA composite films: Effects of acid treatment and filler loading. *Fibers Polym.* **10**, 77–82 (2009). doi:10.1007/s12221-009-0077-x.
43. E.D. Flores, M. Funabashi, and M. Kunioka, Mechanical properties and biomass carbon ratios of poly(butylene succinate) composites filled with starch and cellulose filler using furfural as plasticizer. *J. Appl. Polym. Sci.* **112**, 3410–3417 (2009). doi:10.1002/app.29777.
44. H.-S. Kim, H.-S. Yang, and H.-J. Kim, Biodegradability and mechanical properties of agro-flour-filled polybutylene succinate biocomposites. *J. Appl. Polym. Sci.* **97**, 1513–1521 (2005). doi:10.1002/app.21905.
45. Y. Zhang, C. Yu, P.K. Chu, F. Lv, C. Zhang, J. Ji, R. Zhang, et al., Mechanical and thermal properties of basalt fiber reinforced poly(butylene succinate) composites. *Mater. Chem. Phys.* **133**, 845–849 (2012). doi:10.1016/j.matchemphys.2012.01.105.
46. N. Lin, J. Yu, P.R. Chang, J. Li, and J. Huang, Poly(butylene succinate)-based biocomposites filled with polysaccharide nanocrystals: Structure and properties. *Polym. Compos.* **32**, 472–482 (2011). doi:10.1002/pc.
47. N. Kasyapi, V. Chaudhary, and A.K. Bhowmick, Bionanowhiskers from jute: Preparation and characterization. *Carbohydr. Polym.* **92**, 1116–1123 (2013). doi:10.1016/j.carbpol.2012.10.021.
48. C.J. Chirayil, J. Joy, L. Mathew, M. Mozetic, J. Koetz, and S. Thomas, Isolation and characterization of cellulose nanofibrils from *Helicteres isora* plant. *Ind. Crops Prod.* **59**, 27–34 (2014). doi:10.1016/j.indcrop.2014.04.020.
49. H. Lu, Y. Gui, L. Zheng, and X. Liu, Morphological, crystalline, thermal and physicochemical properties of cellulose nanocrystals obtained from sweet potato residue. *Food Res. Int.* **50**, 121–128 (2013). doi:10.1016/j.foodres.2012.10.013.
50. Z. Lu, L. Fan, H. Zheng, Q. Lu, Y. Liao, and B. Huang, Preparation, characterization and optimization of nanocellulose whiskers by simultaneously ultrasonic wave and microwave assisted. *Bioresour. Technol.* **146**, 82–88 (2013). doi:10.1016/j.biortech.2013.07.047.
51. L. Segal, J.J. Creely, A.E. Martin, and C.M. Conrad, An empirical method for estimating the degree of crystallinity of native cellulose using the X-ray diffractometer. *Text. Res. J.* **29**, 786–794 (1959). doi:10.1177/004051755902901003.
52. K. Oksman, A.P. Mathew, R. Långström, B. Nyström, and K. Joseph, The influence of fibre microstructure on fibre breakage and mechanical properties of natural fibre reinforced polypropylene. *Compos. Sci. Technol.* **69**, 1847–1853 (2009). doi:10.1016/j.compscitech.2009.03.020.
53. S.-Y. Lee, D.J. Mohan, I.-A. Kang, G.-H. Doh, S. Lee, and S.O. Han, Nanocellulose reinforced PVA composite films: Effects of acid treatment and filler loading. *Fibers Polym.* **10**, 77–82 (2009). doi:10.1007/s12221-009-0077-x.
54. E.F. Cerqueira, C.A.R.P. Baptista, and D.R. Mulinari, Mechanical behaviour of polypropylene reinforced sugarcane bagasse fibers composites. *Procedia Eng.* **10**, 2046–2051 (2011). doi:10.1016/j.proeng.2011.04.339.
55. M. Ardanuy, J. Claramunt, J.A. García-Hortal, and M. Barra, Fiber-matrix interactions in cement mortar composites reinforced with cellulosic fibers. *Cellulose*. **18**, 281–289 (2011). doi:10.1007/s10570-011-9493-3.
56. A.I.S. Brigida, V.M.A. Calado, L.R.B. Gonçalves, and M.A.Z. Coelho, Effect of chemical treatments on properties of green coconut fiber. *Carbohydr. Polym.* **79**, 832–838 (2010). doi:10.1016/j.carbpol.2009.10.005.
57. J. Fernández-Bolaños, B. Felizón, A. Heredia, R. Guillén, and A. Jiménez, Characterization of the lignin obtained by alkaline delignification and of the cellulose residue from steam-exploded olive stones. *Bioresour. Technol.* **68**, 121–132 (1999). doi:10.1016/S0960-8524(98)00134-5.
58. J. Li, G. Henriksson, and G. Gellerstedt, Lignin depolymerization/repolymerization and its critical role for delignification of aspen wood by steam explosion. *Bioresour. Technol.* **98**, 3061–3068 (2007). doi:10.1016/j.biortech.2006.10.018.
59. B. Xiao, X. Sun, and R. Sun, Chemical, structural, and thermal characterizations of alkali-soluble lignins and hemicelluloses, and cellulose from maize stems, rye straw, and rice straw. *Polym. Degrad. Stab.* **74**, 307–319 (2001). doi:10.1016/S0141-3910(01)00163-X.
60. C.J. Chirayil, J. Joy, L. Mathew, M. Mozetic, J. Koetz, and S. Thomas, Isolation and characterization of cellulose nanofibrils from *Helicteres isora* plant. *Ind. Crops Prod.* **59**, 27–34 (2014). doi:10.1016/j.indcrop.2014.04.020.
61. C.U. Maheswari, K.O. Reddy, E. Muzenda, B.R. Guduri, and A.V. Rajulu, Extraction and characterization of cellulose microfibrils from agricultural residue – *Cocos nucifera* L. *Biomass Bioenerg.* **46**, 555–563 (2012). doi:10.1016/j.biombioe.2012.06.039.
62. C.F. Liu, F. Xu, J.X. Sun, J.L. Ren, S. Curling, R.C. Sun, P. Fowler, and M.S. Baird, Physicochemical characterization of cellulose from perennial ryegrass leaves

- (*Lolium perenne*). *Carbohydr. Res.* **341**, 2677–2687 (2006). doi:10.1016/j.carres.2006.07.008.
63. M. Sain and S. Panthapulakkal, Bioprocess preparation of wheat straw fibers and their characterization. *Ind. Crops Prod.* **23**, 1–8 (2006). doi:10.1016/j.indcrop.2005.01.006.
64. R. Zuluaga, J.-L. Putaux, A. Restrepo, I. Mondragon, and P. Gañán, Cellulose microfibrils from banana farming residues: isolation and characterization. *Cellulose.* **14**, 585–592 (2007). doi:10.1007/s10570-007-9118-z.
65. Y. Liu, H. Wang, G. Yu, Q. Yu, B. Li, and X. Mu, A novel approach for the preparation of nanocrystalline cellulose by using phosphotungstic acid. *Carbohydr. Polym.* **110**, 415–422 (2014). doi:10.1016/j.carbpol.2014.04.040.
66. K.O. Reddy, C.U. Maheswari, M. Shukla, J.I. Song, and A.V. Rajulu, Tensile and structural characterization of alkali treated Borassus fruit fine fibers. *Compos. Part B Eng.* **44**, 433–438 (2013). doi:10.1016/j.compositesb.2012.04.075.
67. K.O. Reddy, J. Zhang, J. Zhang, and A.V. Rajulu, Preparation and properties of self-reinforced cellulose composite films from Agave microfibrils using an ionic liquid. *Carbohydr. Polym.* **114**, 537–545 (2014). doi:10.1016/j.carbpol.2014.08.054.
68. A. Sonia and K. Priya Dasan, Chemical, morphology and thermal evaluation of cellulose microfibrils obtained from *Hibiscus sabdariffa*. *Carbohydr. Polym.* **92**, 668–674 (2013). doi:10.1016/j.carbpol.2012.09.015.
69. Y. Nishiyama, P. Langan, and H. Chanzy, Crystal structure and hydrogen-bonding system in cellulose I β from synchrotron X-ray and neutron fiber diffraction. *J. Am. Chem. Soc.* **124**, 9074–9082 (2002). doi:10.1021/ja0257319.
70. H. Li, X. Liu, R. Legros, X.T. Bi, C.J. Lim, and S. Sokhansanj, Torrefaction of sawdust in a fluidized bed reactor. *Bioresour. Technol.* **103**, 453–458 (2012). doi:10.1016/j.biortech.2011.10.009.
71. M.K.M. Haafiz, A. Hassan, Z. Zakaria, and I.M. Inuwa, Isolation and characterization of cellulose nanowhiskers from oil palm biomass microcrystalline cellulose. *Carbohydr. Polym.* **103**, 119–125 (2014). doi:10.1016/j.carbpol.2013.11.055.
72. A.W.M. Kahar and H. Ismail, High-density polyethylene/natural rubber blends filled with thermoplastic tapioca starch: Physical and isothermal crystallization kinetics study. *J. Vinyl Addit. Techn.* **22**, 101–199 (2016). doi:10.1002/vnl.
73. S. Pilla, S. Gong, E.O. Neill, L. Yang, and R.M. Rowell, Polylactide-recycled wood fiber composites. *J. Appl. Polym. Sci.* **111**, 37–47 (2008). doi:10.1002/app.
74. H. Han, X. Wang, and D. Wu, Mechanical properties, morphology and crystallization kinetic studies of bio-based thermoplastic composites of poly(butylene succinate) with recycled carbon fiber. *J. Chem. Technol. Biotechnol.* **88**, 1200–1211 (2013). doi:10.1002/jctb.3956.
75. A.G. Facca, M.T. Kortschot, and N. Yan, Predicting the elastic modulus of natural fibre reinforced thermoplastics. *Compos. Part A Appl. Sci. Manuf.* **37**, 1660–1671 (2006). doi:10.1016/j.compositesa.2005.10.006.
76. H. Ibrahim, M. Farag, H. Megahed, and S. Mehanny, Characteristics of starch-based biodegradable composites reinforced with date palm and flax fibers. *Carbohydr. Polym.* **101**, 11–19 (2014). doi:10.1016/j.carbpol.2013.08.051.
77. J.C. Halpin and J. L. Kardos, The Halpin-Tsai equations: A review. *Polym. Eng. Sci.* **16**, 344–352 (1976).
78. S. Elanthikkal, U. Gopalakrishnapanicker, S. Varghese, J.T. Guthrie, and T. Francis, Effect of cellulose whisker content on the properties of poly(ethylene-co-vinyl acetate)/cellulose composites. *Carbohydr. Polym.* **95**, 773–779 (2013). doi:10.1016/j.carbpol.2013.02.039.
79. S.J. Eichhorn, A. Dufresne, M. Aranguren, N.E. Marcovich, J.R. Capadona, S.J. Rowan, et al., Review: Current international research into cellulose nanofibres and nanocomposites. *J. Mater. Sci.* **45**, 1–33 (2009). doi:10.1007/s10853-009-3874-0.